Change-Point Detection With Multivariate Repeated Measures

Serim Han HASER@KAIST.AC.KR

Graduate School of Data Science KAIST Daejeon, 34141, Republic of Korea

Jingru Zhang

JR_ZHANG@FUDAN.EDU.CN School of Data Science

Fudan University Shanghai, 200433, China

Hoseung Song

HOSEUNG@KAIST.AC.KR

Department of Industrial and Systems Engineering KAIST Daejeon, 34141, Republic of Korea

Editor:

Abstract

Graph-based methods have shown particular strengths in change-point detection (CPD) tasks for high-dimensional nonparametric settings. However, existing CPD research has rarely addressed data with repeated measurements or local group structures. A common treatment is to average repeated measurements, which can result in the loss of important within-individual information. In this paper, we propose a new graph-based method for detecting change-points in data with repeated measurements or local structures by incorporating both within-individual and between-individual information. Analytical approximations to the significance of the proposed statistics are derived, enabling efficient computation of p-values for the combined test statistic. The proposed method effectively detects changepoints across a wide range of alternatives, particularly when within-individual differences are present. The new method is illustrated through an analysis of the New York City taxi dataset.

Keywords: High-dimensional data, graph-based method, permutation null distribution, nonparametric

1 Introduction

Change-point detection (CPD) is a fundamental problem in sequential data analysis, where the goal is to identify points in the sequence where the underlying probability distribution changes. CPD has diverse applications in various fields, including healthcare, environmental science, and image or text analysis (Aminikhanghahi and Cook, 2017). Parametric approaches have been widely employed for univariate and low-dimensional data, as they provide effective detection under relatively simple distributional assumptions (see Carlstein et al., 1994; Chen et al., 2000). However, such parametric constraints often limit their applicability to real-world data, particularly in high-dimensional multivariate settings.

To address these limitations, a few nonparametric methods have been proposed. Rankbased methods (Pettitt, 1979; Lombard, 1987; Ross and Adams, 2012; Zhou and Chen, 2025) rely on ordering information to detect distributional shifts. Kernel-based methods (Desobry et al., 2005; Harchaoui et al., 2008; Li et al., 2015; Song and Chen, 2024) capture complex distributional changes by projecting data into a feature space. Inter-point distancebased methods (Matteson and James, 2014; Li, 2020) utilize pairwise distances to detect changes. Graph-based methods (Chen and Zhang, 2015; Shi et al., 2017; Chu and Chen, 2019; Song and Chen, 2022) construct similarity graphs on data points and test for structural changes. Beyond these approaches, other works have addressed related challenges: Saatçi et al. (2010) introduced Gaussian process change-point models that provide a flexible Bayesian nonparametric framework; Wang et al. (2013) developed locality-based test statistics for identifying change-points in graph time series; and Dubey and Müller (2020) proposed a computationally efficient Fréchet change-point method for metric-space-valued data. More recently, machine learning-based approaches have been increasingly developed, with advances fostered by deep learning methods. Jin et al. (2019) proposed a one-class SVM calibration method, and Londschien et al. (2023) developed a random forest framework with theoretical guarantees. Deep neural network-based methods (Ahmadzadeh, 2018; Li et al., 2024) leverage neural architectures to automatically learn representations for effective detection in high-dimensional data.

In many real-world applications, sequential data for CPD involves repeated measurements. For example, in healthcare or medical applications, physical activity data is often collected continuously over multiple days for one person. In such settings, for each time point $i=1,\ldots,n$ with ℓ repeated measures, the observation can be represented as an ℓ -dimensional vector $\mathbf{y}_i=(y_{i1},y_{i2},\ldots,y_{i\ell})^{\mathsf{T}}$. A common approach is to take the average of the repeated measures $\bar{y}_i=(1/\ell)\sum_{j=1}^\ell y_{ij}$, and treat it as a single value for individual i. Another approach is to treat all ℓ measurements as independent features. However, both approaches can lead to a loss of important information, and standard CPD methods may fail to detect meaningful signals arising from the variability among repeated measurements.

The concept of repeated measurements can be extended to local group structures, where similar individuals or temporally adjacent observations exhibit strong correlations. In longitudinal or panel studies, certain local patterns may recur across individuals observed at the same time. Similarly, time series data often exhibit short-term periodic pattern, such as weekly or monthly cycles. Figure 1 illustrates an example where local patterns repeatedly appear over time. Although the global trend appears relatively stable, changes in local structural patterns are observed at specific time points (marked in red). A common practice is to aggregate local patterns, but this may obscure important structural information within the group. Several methods have been proposed to handle repeated measurements or local pattern. Lee and Demets (1991) introduced a group sequential testing procedure based on a linear mixed-effects model to compare rates of change between two treatment groups with repeated measurements, while Horváth and Hušková (2012) proposed a CUSUM-based test for detecting mean shifts in high-dimensional panel data. These methods, however, are parametric and rely on strong model assumptions, which limit their applicability for complex or high-dimensional data.

Recently, Zhang et al. (2022) proposed a graph-based approach for segmentation involving repeated measurements. However, their method does not account for the sequential na-

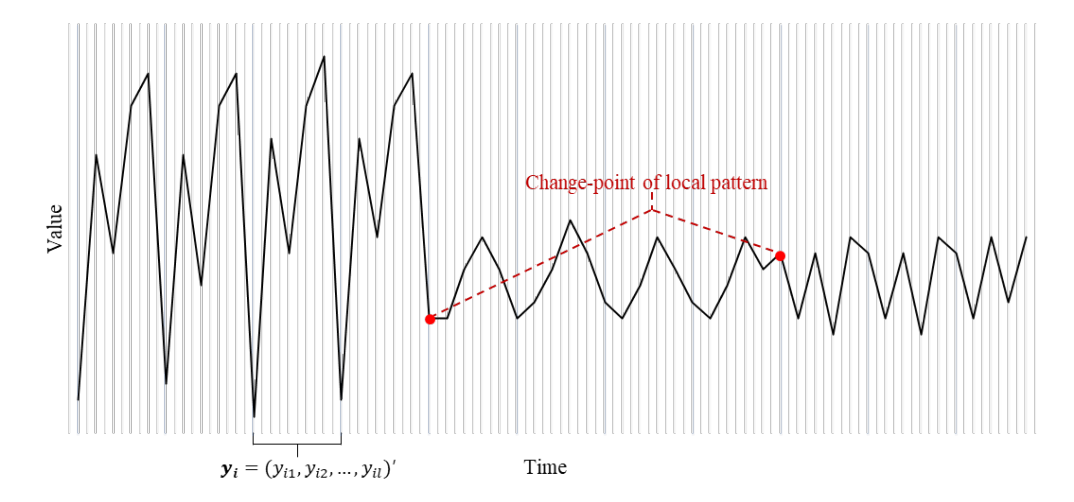


Figure 1: An example of a time series containing changes of local structures. Each vertical stripe represents a time point and the black curve indicates observed values over time. Red markers highlight the time points where local patterns changes.

ture of the data. If a continuous sequence contains strong correlations within local groups, their framework can be extended to CPD settings with such local structures. In these settings, it is essential to develop CPD methods that explicitly account for within-group dependencies and are capable of detecting changes at the level of local patterns.

1.1 Our Contributions

We propose a novel graph-based method for change-point detection in data with repeated measurements or locally structured sequences. Building upon the framework of graph-based statistics with repeated measures introduced by Zhang et al. (2022), we extend the two-sample test setting to the change-point detection scenario. Specifically, we construct a maxtype combination of within-individual and between-individual statistics, enabling the new test to detect change-points driven by either type of structural change. We also establish the limiting distributions of the proposed stochastic processes and derive analytical p-value approximations with the implementation of skewness correction, facilitating application to large datasets. The codes for reproducing simulation results are available at https://github.com/haser66/gSeg_repeated.

The organization of the paper is as follows. In Section 2, we propose three new scan statistics to accommodate repeated measurements and local group structures in the sequence. The asymptotic behavior of the new scan statistics, the analytical p-value approximations, and a proposed test are presented in Section 3. The new test performs well under a wide range of alternatives involving repeated measures, as shown in Section 4 through extensive simulations and in Section 5 with the New York City taxi dataset. The details of proofs of theorems are deferred to the Appendix.

2 New Scan Statistics

We consider a sequence of independent observations

$$\mathbf{y}_i = (y_{i1}, y_{i2}, \dots, y_{i\ell})^T, \quad i = 1, \dots, n,$$

where each $y_{ij} \in \mathbb{R}^d$, $j = 1, ..., \ell$, represents a d-dimensional measurement taken at the j-th repeated measure, and ℓ denotes the number of repeated measures for each individual. Thus, \mathbf{y}_i can be viewed as a sequence of ℓ vectors in \mathbb{R}^d , equivalently represented as an $\ell \times d$ matrix. We aim to test the null hypothesis

$$H_0: \mathbf{y}_i \sim F_0, \quad i = 1, \dots, n, \tag{1}$$

against the single change-point alternative

$$H_1: \exists \ 1 \le \tau < n, \quad \mathbf{y}_i \sim \begin{cases} F_0 & \text{if } i \le \tau, \\ F_1 & \text{otherwise.} \end{cases}$$
 (2)

To preserve the structure of repeated measurements in the graph-based approach, we construct a similarity graph G, such as a minimum spanning tree¹ (MST) or nearest neighbor graph (NNG), based on all repeated measurements across individuals. In particular, we adopt the k-MST² algorithm to construct the graph on $n \times \ell$ nodes, representing n individuals with ℓ repeated measures per individual. Following the recommendation of Chen et al. (2018), we set k=9, thereby using the 9-MST as the similarity graph. We then divide G into two disjoint subgraphs: between-individual graph $G_{\rm out}$ and within-individual graph $G_{\rm in}$. $G_{\rm out}$ contains edges connecting nodes from different individuals and $G_{\rm in}$ contains edges connecting nodes belonging to the same individual.

We define the indicator function for any node i observed after a time point t as $g_i(t) = I_{i>t}$. For an edge $e = (i, j) \in G$, the edge type $J_e(t)$ is given by

$$J_e(t) = \begin{cases} 0, & \text{if } g_i(t) \neq g_j(t), \\ 1, & \text{if } g_i(t) = g_j(t) = 0, \\ 2, & \text{if } g_i(t) = g_i(t) = 1. \end{cases}$$

For any candidate value t of τ , we define

$$R_{\text{out},k}(t) = \sum_{e \in G_{\text{out}}} I_{J_e(t)=k}, \quad R_{\text{in},k}(t) = \sum_{e \in G_{\text{in}}} I_{J_e(t)=k}, \quad k = 1, 2.$$
 (3)

Accordingly, $R_{\text{out},1}(t)$ and $R_{\text{in},1}(t)$ represent the numbers of between-individual edges and within-individual edges connecting observations prior to t, respectively. Similarly, $R_{\text{out},2}(t)$ and $R_{\text{in},2}(t)$ denote the corresponding numbers of edges connecting observations after t. Figure 2 illustrates the decomposition of G into G_{out} and G_{in} . Edges connecting nodes

^{1.} An MST is a spanning tree that connects all observations minimizing the sum of the distances of edges.

^{2.} A k-MST is the union of the first through the kth MSTs. The 1st MST is the usual minimum spanning tree, and each jth MST (j > 1) connects all observations and minimizes the sum of the distances of all edges without using any edge from the previous 1st MST, \cdots , and (j - 1)th MST.

prior to t are depicted in blue tones, while those connecting nodes after t are red-toned. Dark blue and dark red lines represent the edges between different individuals and thus belong to G_{out} . Light blue and light red lines indicate edges within the same individual and are included in G_{in} . Gray lines correspond to the edges connecting the nodes before and after t.

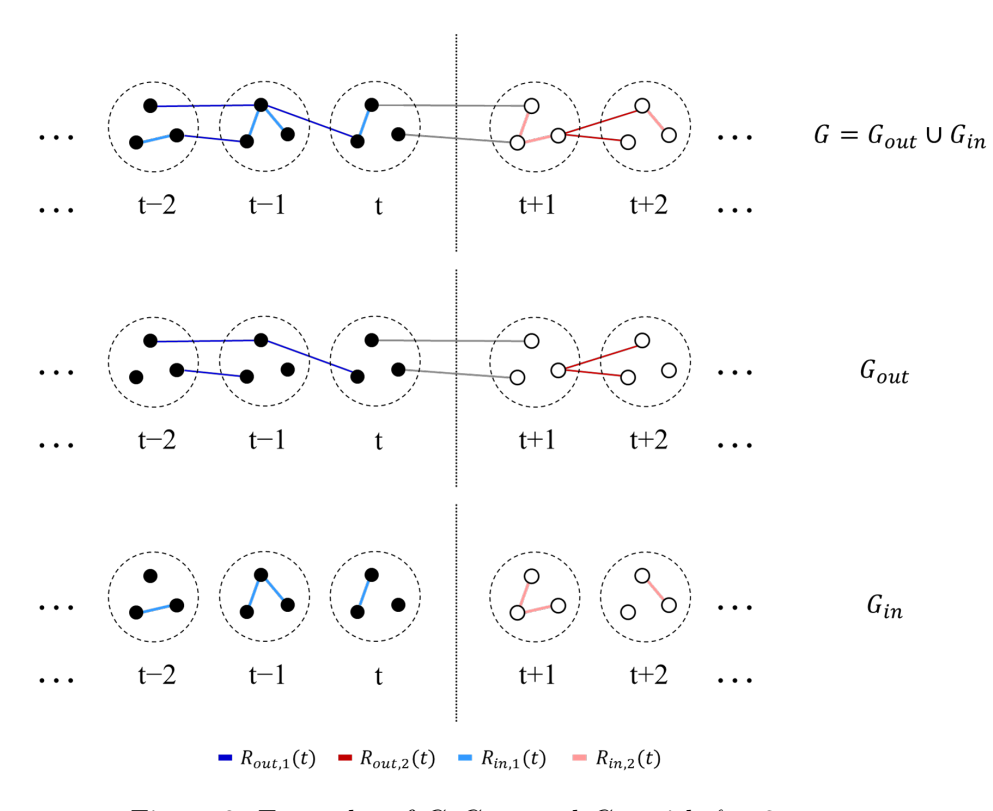


Figure 2: Examples of G, G_{out} , and G_{in} with $\ell = 3$.

We evaluate the extent to which the observed test statistic deviates from its permutation null distribution. Under H_0 , the n individuals are permuted, with each permutation having equal probability 1/n!. In this procedure, the repeated measurements of the same individual are treated as a single unit and are permuted jointly. In other words, if an individual \mathbf{y}_i is assigned to a particular group in a given permutation, all of its repeated measurements are simultaneously assigned to that group. Unless otherwise specified, we use P, E, Var, and Cov to denote probability, expectation, variance, and covariance under the permutation null distribution, respectively.

Let |G|, $|G_{\text{out}}|$, and $|G_{\text{in}}|$ be the number of edges in graphs G, G_{out} , and G_{in} , respectively. As illustrated in Figure 2, the set G_{out} consists of three types of edges: dark blue edges $(R_{\text{out},1}(t))$, dark red edges $(R_{\text{out},2}(t))$, and the remaining gray edges. Since the number of gray edges is determined by $|G_{\text{out}}| - R_{\text{out},1}(t) - R_{\text{out},2}(t)$, the pair $(R_{\text{out},1}(t), R_{\text{out},2}(t))$ fully characterizes the information in G_{out} . Similarly, the set G_{in} consists of light blue edges $(R_{\text{in},1}(t))$ and light red edges $(R_{\text{in},2}(t))$. Since $R_{\text{in},2}(t)$ is determined by $|G_{\text{in}}| - R_{\text{in},1}(t)$, it is sufficient to use $R_{\text{in},1}(t)$ alone to capture all the information contained in G_{in} .

To capture changes in between-individual connectivity, we consider two test statistics $R_{\text{out},w}(t)$ and $R_{\text{out},d}(t)$, which are linear combinations of $R_{\text{out},1}(t)$ and $R_{\text{out},2}(t)$,

$$R_{\text{out},w}(t) = \frac{(n-t-1)R_{\text{out},1}(t) + (t-1)R_{\text{out},2}(t)}{n-2},$$

$$R_{\text{out},d}(t) = R_{\text{out},1}(t) - R_{\text{out},2}(t).$$

We would expect $R_{\text{out},w}(t)$ to detect location changes, whereas $R_{\text{out},d}(t)$ would be sensitive to scale changes. Taking into account changes in within-individual connectivity as well, we employ $R_{\text{out},w}(t)$, $R_{\text{out},d}(t)$, and $R_{\text{in},1}(t)$ to comprehensively capture the change-point signal in repeated measurements. The corresponding standardized versions of these statistics are

$$Z_{\mathrm{out},w}(t) = \frac{R_{\mathrm{out},w}(t) - \mu_{\mathrm{out},w}(t)}{\sigma_{\mathrm{out},w}(t)}, \ Z_{\mathrm{out},d}(t) = \frac{R_{\mathrm{out},d}(t) - \mu_{\mathrm{out},d}(t)}{\sigma_{\mathrm{out},d}(t)}, \ Z_{\mathrm{in}}(t) = \frac{R_{\mathrm{in},1}(t) - \mu_{\mathrm{in}}(t)}{\sigma_{\mathrm{in}}(t)},$$

where

$$\begin{split} &\mu_{\mathrm{out},w}(t) = \mathsf{E}(R_{\mathrm{out},w}(t)), \qquad \mu_{\mathrm{out},d}(t) = \mathsf{E}(R_{\mathrm{out},d}(t)), \qquad \mu_{\mathrm{in}}(t) = \mathsf{E}(R_{\mathrm{in},1}(t)), \\ &\sigma_{\mathrm{out},w}(t) = \sqrt{\mathsf{Var}(R_{\mathrm{out},w}(t))}, \quad \sigma_{\mathrm{out},d}(t) = \sqrt{\mathsf{Var}(R_{\mathrm{out},d}(t))}, \quad \sigma_{\mathrm{in}}(t) = \sqrt{\mathsf{Var}(R_{\mathrm{in},1}(t))}. \end{split}$$

Under the alternative hypothesis, $Z_{\text{out},w}(t)$ tends to be large for location shifts in between-individuals, while $|Z_{\text{out},d}(t)|$ tends to be large for scale changes in between-individuals. $|Z_{\text{in}}(t)|$ becomes large for changes that occur within individuals. Considering these three statistics together, a wide range of distributional changes can be effectively detected.

We define a symmetric matrix $D=(D_{uv})_{n\times n}$, where D_{uv} is the number of edges between individuals u and v in G. For each individual u, we denote by $D_u=\sum_{v\neq u}D_{uv}$ the total number of edges that connect individual u to others. The following lemma provides analytic expressions for E, Var, and Cov without explicitly performing permutations.

Lemma 1 Under the permutation null distribution, we have

$$\begin{split} \textit{E}(R_{out,1}(t)) &= \frac{t(t-1)}{n(n-1)} |G_{out}|, \quad \textit{E}(R_{out,2}(t)) = \frac{(n-t)(n-t-1)}{n(n-1)} |G_{out}|, \\ \textit{E}(R_{in,1}(t)) &= \frac{t}{n} |G_{in}|, \\ \textit{Var}(R_{out,1}(t)) &= \frac{t(t-1)(n-t)(n-t-1)}{n(n-1)(n-2)(n-3)} \\ &\qquad \times \left\{ \sum_{u \neq v} \frac{D_{uv}^2}{2} + \frac{t-2}{n-t-1} \left(\sum_{u} D_u^2 - \frac{4}{n} |G_{out}|^2 \right) - \frac{2}{n(n-1)} |G_{out}|^2 \right\}, \\ \textit{Var}(R_{out,2}(t)) &= \frac{t(t-1)(n-t)(n-t-1)}{n(n-1)(n-2)(n-3)} \\ &\qquad \times \left\{ \sum_{u \neq v} \frac{D_{uv}^2}{2} + \frac{n-t-2}{t-1} \left(\sum_{u} D_u^2 - \frac{4}{n} |G_{out}|^2 \right) - \frac{2}{n(n-1)} |G_{out}|^2 \right\}, \end{split}$$

$$\begin{split} \textit{Var}(R_{in,1}(t)) &= \frac{t(n-t)}{n(n-1)} \left(\sum_{u} D_{uu}^2 - \frac{|G_{in}|^2}{n} \right), \\ \textit{Cov}(R_{out,1}(t), R_{out,2}(t)) &= \frac{t(t-1)(n-t)(n-t-1)}{n(n-1)(n-2)(n-3)} \\ &\qquad \times \left\{ \sum_{u \neq v} \frac{D_{uv}^2}{2} - \left(\sum_{u} D_u^2 - \frac{4}{n} |G_{out}|^2 \right) - \frac{2}{n(n-1)} |G_{out}|^2 \right\}, \\ \textit{Cov}(R_{out,1}(t), R_{in,1}(t)) &= \frac{t(t-1)(n-t)}{n(n-1)(n-2)} \left(\sum_{u=1}^n D_{uu} D_u - \frac{2}{n} |G_{in}| |G_{out}| \right), \\ \textit{Cov}(R_{out,2}(t), R_{in,1}(t)) &= -\frac{t(n-t)(n-t-1)}{n(n-1)(n-2)} \left(\sum_{u=1}^n D_{uu} D_u - \frac{2}{n} |G_{in}| |G_{out}| \right). \end{split}$$

The proof is provided in Appendix ??.

Based on the results of Lemma 1, each statistic is standardized such that its expectation equals zero and variance equals one. The covariances are given by $Cov(Z_{\text{out},w}(t), Z_{\text{out},d}(t)) = 0$ and $Cov(Z_{\text{out},w}(t), Z_{\text{in}}(t)) = 0$. Note that the covariance between $Z_{\text{out},d}(t)$ and $Z_{\text{in}}(t)$ is not generally zero; we will address this correlation in Section 3.5.

3 Asymptotics of the Scan Statistics and the New Test

To conduct change-point testing, it is necessary to evaluate the significance level of the proposed scan statistics. For this purpose, we combine $Z_{\text{out},w}(t), |Z_{\text{out},d}(t)|$, and $|Z_{\text{in}}(t)|$ into a unified scan statistic and propose a new test based on its tail probability. While permutation procedures remain feasible for small sample sizes, it is often time-consuming when n is large. Hence, we develop analytic expressions that enable fast and practical implementation. Specifically, we derive the asymptotic distribution of the scan statistics and then improve the accuracy through skewness correction.

3.1 Asymptotic Null Distributions of the Basic Processes

In this section, we first derive the limiting distributions of $\{Z_{\text{out},w}([nu]): 0 < u < 1\}$, $\{Z_{\text{out},d}([nu]): 0 < u < 1\}$, and $\{Z_{\text{in}}([nu]): 0 < u < 1\}$. Here, [x] denotes the largest integer that is no larger than x. Before proceeding, we specify the notation and assumptions of the setting. Let C_u denote the set of repeated measurements from individual u. For an edge $e = (i, j) \in G_{\text{out}}$, where $i \in C_u$, $j \in C_v$, and $u \neq v$, let

$$A_{\text{out},e} = \{e\} \cup \{e' = (k,\ell) \in G_{\text{out}} \mid k \in C_u \cup C_v \text{ or } \ell \in C_u \cup C_v\}$$
$$\cup \{e'' = (k,\ell) \in G_{\text{out}} \mid k,\ell \in C_u \cup C_v\},$$

and for an edge $e = (i, j) \in G_{in}$ with $i, j \in C_u$, define

$$A_{\text{in},e} = \{e' = (k,\ell) \in G_{\text{out}} \mid k \in C_u \text{ or } \ell \in C_u\} \cup \{e' = (\ell,k) \in G_{\text{in}} \mid k,\ell \in C_u\}.$$

We then set

$$A_e = \begin{cases} A_{\text{out},e}, & \text{if } e \in G_{\text{out}}, \\ A_{\text{in},e}, & \text{if } e \in G_{\text{in}}. \end{cases}$$

The corresponding set B_e is defined in a similar way:

$$B_{\text{out},e} = \bigcup_{\tilde{e} \in A_{\text{out},e}} A_{\tilde{e}}, \qquad B_{\text{in},e} = \bigcup_{\tilde{e} \in A_{\text{in},e}} A_{\tilde{e}}, \qquad B_e = \begin{cases} B_{\text{out},e}, & \text{if } e \in G_{\text{out}}, \\ B_{\text{in},e}, & \text{if } e \in G_{\text{in}}. \end{cases}$$

We assume t = O(n), n - t = O(n) and $\ell = O(1)$. Throughout, we write $a_n = O(b_n)$ when a_n and b_n are of the same order, and write $a_n = o(b_n)$ when a_n is of smaller order than b_n . We proceed to introduce the following conditions.

Condition 1 $|G_{out}| = O(n)$, $|G_{in}| = O(n)$.

Condition 2
$$\sum_{u} D_u^2 - \frac{4|G_{out}|^2}{n} = O(n), \sum_{u} D_{uu}^2 - \frac{|G_{in}|^2}{n} = O(n).$$

Condition 3
$$\sum_{e \in G_{out}} |A_{out,e}| |B_{out,e}| = o(n^{1.5}).$$

Remark 2 Condition 1 requires that the numbers of edges in G_{out} and G_{in} grow on the same order as n and can be easily satisfied with an appropriate choice of G. Condition 2 ensures that $(R_{out,1}(t), R_{out,2}(t), R_{in,1}(t))^{\top}$ does not degenerate asymptotically. For example, since

$$\sum_{u} D_{u}^{2} - \frac{4|G_{out}|^{2}}{n} = \sum_{u} \left(D_{u} - \frac{2|G_{out}|}{n} \right)^{2}, \quad \sum_{u} D_{uu}^{2} - \frac{|G_{in}|^{2}}{n} = \sum_{u} \left(D_{uu} - \frac{|G_{in}|}{n} \right)^{2},$$

if $D_u - 2|G_{out}|/n = O(1)$ and $D_{uu} - |G_{in}|/n = O(1)$, Condition 2 is satisfied. Condition 3 requires that the graph has no large hub or a cluster of small hubs, where a hub is a node with a large degree. Similar conditions appears in the context of graph-based statistics for independent observations (Chen and Friedman, 2017 and Chen et al., 2018).

Remark 3 The condition $|G_{in}| = O(n)$ requires that repeated measurements contain sufficient common information, ensuring that within-individual edges grow at a meaningful rate and can be explored by our test statistic $Z_{in}(t)$. We also assume $\ell = O(1)$, i.e., as $n \to \infty$, the number of repeated measurements per individual remains bounded. This prevents a large hub from dominating the majority of edges in G and ensures that the regularity conditions, such as Condition 3, hold.

Theorem 4 Under Conditions 1–3, as $n \to \infty$,

- 1. $\{Z_{out,w}([nu]): 0 < u < 1\}$ and $\{Z_{out,d}([nu]): 0 < u < 1\}$ converge to independent Gaussian processes in finite dimensional distributions, which we denote as $\{Z_{out,w}^*(u): 0 < u < 1\}$ and $\{Z_{out,d}^*(u): 0 < u < 1\}$, respectively.
- 2. $\{Z_{out,w}([nu]): 0 < u < 1\}$ and $\{Z_{in}([nu]): 0 < u < 1\}$ converge to independent Gaussian processes in finite dimensional distributions, denoted by $\{Z_{out,w}^*(u): 0 < u < 1\}$ and $\{Z_{in}^*(u): 0 < u < 1\}$, respectively.

The proof is provided in Appendix ??.

Let $\rho_{\mathrm{out},w}^*(u,v) = \mathsf{Cov}(Z_{\mathrm{out},w}^*(u),Z_{\mathrm{out},w}^*(v)), \ \rho_{\mathrm{out},d}^*(u,v) = \mathsf{Cov}(Z_{\mathrm{out},d}^*(u),Z_{\mathrm{out},d}^*(v))$ and $\rho_{\mathrm{in}}^*(u,v) = \mathsf{Cov}(Z_{\mathrm{in}}^*(u),Z_{\mathrm{in}}^*(v)).$ The exact covariance functions of the limiting Gaussian processes $\{Z_{\mathrm{out},w}^*(u):\ 0 < u < 1\},\ \{Z_{\mathrm{out},d}^*(u):\ 0 < u < 1\},\ and\ \{Z_{\mathrm{in}}^*(u):\ 0 < u < 1\}$ are stated in the following theorem.

Theorem 5 The exact expressions for $\rho_{out,w}^*(u,v)$, $\rho_{out,d}^*(u,v)$ and $\rho_{in}^*(u,v)$ are

$$\rho_{out,w}^*(u,v) = \frac{(u \wedge v)(1 - (u \vee v))}{(u \vee v)(1 - (u \wedge v))},$$

$$\rho_{out,d}^*(u,v) = \rho_{in}^*(u,v) = \frac{(u \wedge v)(1 - (u \vee v))}{\sqrt{(u \wedge v)(1 - (u \wedge v))(u \vee v)(1 - (u \vee v))}},$$

where $u \wedge v = \min(u, v)$ and $u \vee v = \max(u, v)$.

The proof of Theorem 5 can be found in Appendix ??.

3.2 Analytical P-value Approximation

Based on Theorems 4 and 5, we approximate the tail probabilities through the Woodroofe's method (Woodroofe, 1976, 1978) and Siegmund's method (Siegmund, 1988, 1992). Specifically, following similar arguments in the proof for Proposition 3.4 in Chen and Zhang (2015), when Conditions 1–3 hold, $n, b, n_0, n_1 \to \infty$ in a way such that for some $b_0 > 0$ and $0 < x_0 < x_1 < 1, b/\sqrt{n} \to b_0, n_0/n \to x_0$ and $n_1/n \to x_1$, as $n \to \infty$, we have

$$\mathsf{P}\left(\max_{n_0 \leq t \leq n_1} Z^*_{\mathrm{out},w}(t/n) > b\right) \sim b\phi(b) \int_{x_0}^{x_1} h^*_{\mathrm{out},w}(x) \ \nu\left(b_0 \sqrt{2h^*_{\mathrm{out},w}(x)}\right) \ dx,$$

$$\mathsf{P}\left(\max_{n_0 \leq t \leq n_1} \left| Z_{\mathrm{out},d}^*(t/n) \right| > b \right) \sim 2b\phi(b) \int_{x_0}^{x_1} h_{\mathrm{out},d}^*(x) \ \nu\left(b_0 \sqrt{2h_{\mathrm{out},d}^*(x)}\right) \ dx,$$

$$\mathsf{P}\left(\max_{n_0 \le t \le n_1} |Z_{\rm in}^*(t/n)| > b\right) \sim 2b\phi(b) \int_{x_0}^{x_1} h_{\rm in}^*(x) \ \nu\left(b_0 \sqrt{2h_{\rm in}^*(x)}\right) \ dx,$$

where

$$h_{\text{out},w}^{*}(x) = \lim_{u \nearrow x} \frac{\partial \rho_{\text{out},w}^{*}(u,x)}{\partial u} = -\lim_{u \searrow x} \frac{\partial \rho_{\text{out},w}^{*}(u,x)}{\partial u},$$

$$h_{\text{out},d}^{*}(x) = \lim_{u \nearrow x} \frac{\partial \rho_{\text{out},d}^{*}(u,x)}{\partial u} = -\lim_{u \searrow x} \frac{\partial \rho_{\text{out},d}^{*}(u,x)}{\partial u},$$

$$h_{\text{in}}^{*}(x) = \lim_{u \nearrow x} \frac{\partial \rho_{\text{in}}^{*}(u,x)}{\partial u} = -\lim_{u \searrow x} \frac{\partial \rho_{\text{in}}^{*}(u,x)}{\partial u}.$$

Here, $\nu(x)$ can be numerically approximated as

$$\nu(x) \approx \frac{(2/x)(\Phi(x/2) - 0.5)}{(x/2)\Phi(x/2) + \phi(x/2)}$$

by Siegmund and Yakir (2007), where $\Phi(\cdot)$ and $\phi(\cdot)$ are the standard normal cumulative density function and standard normal density function, respectively. It can be shown that

$$h_{\text{out},w}^*(x) = \frac{1}{x(1-x)}, \quad h_{\text{out},d}^*(x) = h_{\text{in}}^*(x) = \frac{1}{2x(1-x)}.$$

Based on the above results, we can approximate the tail probabilities by

$$\mathsf{P}\left(\max_{n_0 \le t \le n_1} Z_{\mathrm{out},w}(t) > b\right) \approx b\phi(b) \int_{x_0}^{x_1} h_{\mathrm{out},w}^*(x) \ \nu\left(b\sqrt{2h_{\mathrm{out},w}^*(x)/n}\right) \ dx,\tag{4}$$

$$\mathsf{P}\left(\max_{n_0 \leq t \leq n_1} |Z_{\mathrm{out},d}(t)| > b\right) \approx 2b\phi(b) \int_{x_0}^{x_1} h_{\mathrm{out},d}^*(x) \ \nu\left(b\sqrt{2h_{\mathrm{out},d}^*(x)/n}\right) \, dx, \tag{5}$$

$$\mathsf{P}\left(\max_{n_0 \leq t \leq n_1} |Z_{\mathrm{in}}(t)| > b\right) \approx 2b\phi(b) \int_{x_0}^{x_1} h_{\mathrm{in}}^*(x) \ \nu\left(b\sqrt{2h_{\mathrm{in}}^*(x)/n}\right) \ dx. \tag{6}$$

Remark 6 In practice, when approximating the tail probabilities, we use $h_{out,w}(n,x)$ in place of $h_{out,w}^*(x)$, where $h_{out,w}(n,x)$ is the finite-sample equivalent of $h_{out,w}^*(x)$. That is,

$$h_{out,w}(n,x) = n \lim_{s \nearrow nx} \frac{\partial \rho_{out,w}(s,nx)}{\partial s},$$

with $\rho_{out,w}(s,t) := Cov(Z_{out,w}(s), Z_{out,w}(t))$. The explicit expression for $h_{out,w}(n,x)$ can also be derived and simplified to be

$$h_{out,w}(n,x) = \frac{(n-1)(2nx^2 - 2nx + 1)}{2x(1-x)(n^2x^2 - n^2x + n - 1)}.$$

It is clear from the above expression that $h_{out,w}(n,x)$ does not depend on the graph G as well. Also, it is easy to show that $\lim_{n\to\infty} h_{out,w}(n,x) = h_{out,w}^*(x)$.

The finite-sample equivalent version of $h_{out,d}^*(x)$ has the same closed-form expression as $h_{out,d}^*(x)$. This can be written as

$$h_{out,d}(n,x) = n \lim_{s \nearrow nx} \frac{\partial \operatorname{Cov}(Z_{out,d}(s), Z_{out,d}([nx]))}{\partial s} = \frac{1}{2x(1-x)}.$$

Similarly, $h_{in}(x)$ can be expressed in the same way as $h_{out,d}(x)$. That is, $h_{in}(n,x) = 1/(2x(1-x))$.

3.3 Skewness Correction

As discussed in Chen and Zhang (2015) and Chu and Chen (2019), the analytical approximations of the tail probabilities (4)–(6) can be improved by skewness correction as n_0 and n_1 are close to the two ends, particularly in high-dimensional settings or when the similarity graph contains hubs. This arises because, when t/n is close to 0 or 1, $Z_{\text{out},w}(t)$, $Z_{\text{out},d}(t)$, and $Z_{\text{in}}(t)$ slowly converge to Gaussian processes. Figure 3 displays the skewness of these statistics for a sequence of 1000 individuals, each with 5 repeated measures, generated from the multivariate Gaussian distribution. It can be clearly seen that $Z_{\text{out},w}(t)$ is strongly right-skewed near both ends of the sequence, whereas $Z_{\text{out},d}(t)$ and $Z_{\text{in}}(t)$ are right-skewed for small t and left-skewed for large t.

To address this issue, since the skewness depends on the value of t, we employ the procedure described in Chen and Zhang (2015). Let $\gamma_{\text{out},w}(t) = \mathsf{E}(Z_{\text{out},w}^3(t))$, $\gamma_{\text{out},d}(t) = \mathsf{E}(Z_{\text{out},d}^3(t))$, and $\gamma_{\text{in}}(t) = \mathsf{E}(Z_{\text{in}}^3(t))$. The analytical p-value approximations after skewness

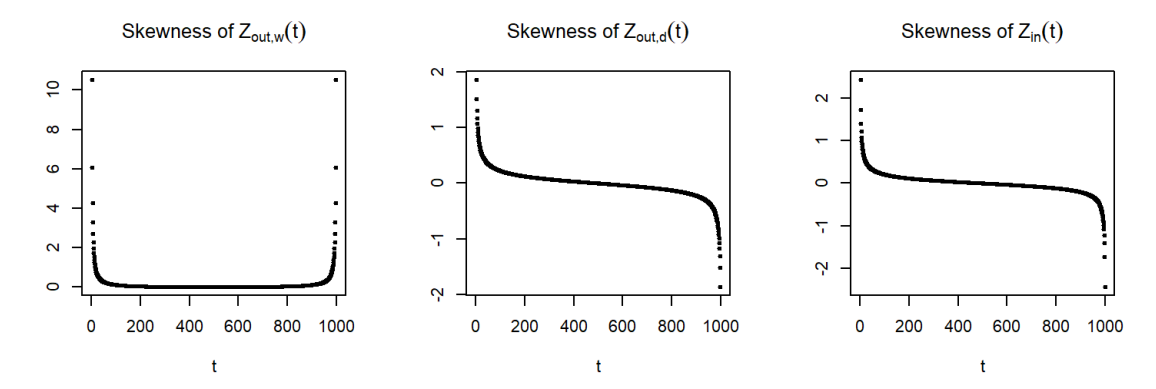


Figure 3: Plots of skewness $\gamma_{\text{out},w}(t)$, $\gamma_{\text{out},d}(t)$ and $\gamma_{\text{in}}(t)$ against t with MST for a sequence of 1000 points randomly generated from the 50-dimensional multivariate Gaussian distribution with $\ell=5$.

correction are

$$\mathsf{P}\left(\max_{n_0 \le t \le n_1} Z_{\mathrm{out},w}(t) > b\right) \approx b\phi(b) \int_{n_0/n}^{n_1/n} K_{\mathrm{out},w}(nx) h_{\mathrm{out},w}(n,x) \nu\left(b\sqrt{2h_{\mathrm{out},w}(n,x)/n}\right) dx, \tag{7}$$

$$\mathsf{P}\left(\max_{n_0 \le t \le n_1} |Z_{\mathrm{out},d}(t)| > b\right) \approx 2b\phi(b) \int_{n_0/n}^{n_1/n} K_{\mathrm{out},d}(nx) h_{\mathrm{out},d}(n,x) \nu\left(b\sqrt{2h_{\mathrm{out},d}(n,x)/n}\right) dx, \tag{8}$$

$$\mathsf{P}\left(\max_{n_0 \le t \le n_1} |Z_{\mathrm{in}}(t)| > b\right) \approx 2b\phi(b) \int_{n_0/n}^{n_1/n} K_{\mathrm{in}}(nx) h_{\mathrm{in}}(n,x) \nu\left(b\sqrt{2h_{\mathrm{in}}(n,x)/n}\right) dx, \tag{9}$$

where

$$K_{\text{out},w}(t) = \frac{\exp\left(\frac{1}{2}(b - \hat{\theta}_{b,w}(t))^2 + \frac{1}{6}\gamma_{\text{out},w}(t)\hat{\theta}_{b,w}(t)^3\right)}{\sqrt{1 + \gamma_{\text{out},w}(t)\hat{\theta}_{b,w}(t)}} \quad \text{with } \hat{\theta}_{b,w}(t) = \frac{-1 + \sqrt{1 + 2\gamma_{\text{out},w}(t)b}}{\gamma_{\text{out},w}(t)},$$

$$K_{\text{out},d}(t) = \frac{\exp\left(\frac{1}{2}(b - \hat{\theta}_{b,d}(t))^2 + \frac{1}{6}\gamma_{\text{out},d}(t)\hat{\theta}_{b,d}(t)^3\right)}{\sqrt{1 + \gamma_{\text{out},d}(t)\hat{\theta}_{b,d}(t)}} \quad \text{with } \hat{\theta}_{b,d}(t) = \frac{-1 + \sqrt{1 + 2\gamma_{\text{out},d}(t)b}}{\gamma_{\text{out},d}(t)},$$

$$K_{\text{in}}(t) = \frac{\exp\left(\frac{1}{2}(b - \hat{\theta}_{b,\text{in}}(t))^2 + \frac{1}{6}\gamma_{\text{in}}(t)\hat{\theta}_{b,\text{in}}(t)^3\right)}{\sqrt{1 + \gamma_{\text{in}}(t)\hat{\theta}_{b,\text{in}}(t)}} \quad \text{with } \hat{\theta}_{b,\text{in}}(t) = \frac{-1 + \sqrt{1 + 2\gamma_{\text{in}}(t)b}}{\gamma_{\text{in}}(t)}.$$

The only unknown quantities in the above expressions are $\gamma_{\text{out},w}(t)$, $\gamma_{\text{out},d}(t)$, and $\gamma_{\text{in}}(t)$. Since

$$\mathsf{E}(Z_{\mathrm{out},w}^3(t)) = \frac{\mathsf{E}(R_{\mathrm{out},w}^3(t)) - 3\mu_{\mathrm{out},w}(t)\sigma_{\mathrm{out},w}^2(t) - \mu_{\mathrm{out},w}^3(t)}{\sigma_{\mathrm{out},w}^3(t)},$$

$$\begin{split} \mathsf{E}(Z_{\mathrm{out},d}^3(t)) &= \frac{\mathsf{E}(R_{\mathrm{out},d}^3(t)) - 3\mu_{\mathrm{out},d}(t)\sigma_{\mathrm{out},d}^2(t) - \mu_{\mathrm{out},d}^3(t)}{\sigma_{\mathrm{out},d}^3(t)}, \\ \mathsf{E}(Z_{\mathrm{in}}^3(t)) &= \frac{\mathsf{E}(R_{\mathrm{in},1}^3(t)) - 3\mu_{\mathrm{in}}(t)\sigma_{\mathrm{in}}^2(t) - \mu_{\mathrm{in}}^3(t)}{\sigma_{\mathrm{in}}^3(t)}, \end{split}$$

it suffices to obtain the analytic expressions for the third moments of $R_{\text{out},w}(t)$, $R_{\text{out},d}(t)$, and $R_{\text{in},1}(t)$, whose analytic forms are provided in Appendix ??.

3.4 Assessment of P-value Approximations under Finite n

To assess the accuracy of the p-value approximations under finite samples, we compare the critical values from the analytical approximations with the critical values obtained via permutations. We set the number of individuals to n=200 and the number of repeated measurements to $\ell=5$. Under the null hypothesis, data are generated from the multivariate Gaussian distribution with three different dimensions d=10, 50, and 100, corresponding to (C1), (C2), and (C3) in Tables 1 and 2. The tables present the critical values at 0.05 significance level for $n_0=0.1n$ and $n_0=0.05n$ with $n_1=n-n_0$, respectively. "A1" denotes the analytic critical values without skewness correction, which do not depend on the graph structure. "A2" and "Per" denote the skewness-corrected analytic critical values and the critical values obtained from 10,000 random permutations, respectively. We construct the similarity graph using 9-MST and use two randomly generated graphs for each configuration to calculate the test statistics and associated critical values.

Table 1: Critical values at 0.05 significance level. $n = 200, \ \ell = 5, \ n_0 = 0.05n$.

	$Z_{\mathrm{out},w}(t)$	$ Z_{\mathrm{out},d}(t) $	$ Z_{\mathrm{in}}(t) $
A1	2.986	3.032	3.032

		$Z_{\mathrm{out},w}(t)$		$ Z_{\mathrm{out},d}(t) $		$ Z_{ m in}(t) $	
		A2	Per	A2	Per	A2	Per
(C1)	d = 10	3.192 3.209	3.281 3.343	3.033 3.033	3.029 3.024	3.074 3.073	3.103 3.082
(C2)	d = 50	3.269 3.265	3.431 3.479	3.033 3.033	3.044 3.032	3.063 3.073	3.019 3.136
(C3)	d = 100	3.331 3.336	3.573 3.529	3.033 3.059	3.012 3.056	3.090 3.064	3.097 3.037

Overall, our p-value approximation performs well, and skewness correction yields more accurate and stable approximations. Across settings, the skewness-corrected critical values closely track the permutation benchmarks, and the agreement further improves when the minimum window size increases (e.g., $n_0 = 0.1n$). Concordance is particularly strong for $|Z_{\text{out},d}(t)|$ and $|Z_{\text{in}}(t)|$, which exhibit negligible differences from permutations. Even for $Z_{\text{out},w}(t)$, whose distribution is highly skewed, the skewness-corrected critical values remain close to the permutation-based critical values. Similar results under the log-normal distribution are provided in Appendix ??.

Table 2: Critical values at 0.05 significance level. $n = 200, \ \ell = 5, \ n_0 = 0.1n$.

	$Z_{\mathrm{out},w}(t)$	$ Z_{\mathrm{out},d}(t) $	$ Z_{\rm in}(t) $
A1	2.900	2.942	2.942

		$Z_{\mathrm{out},w}(t)$		$ Z_{\mathrm{out},d}(t) $		$ Z_{\mathrm{in}}(t) $	
		A2	Per	A2	Per	A2	Per
(C1)	d = 10	3.085 3.092	3.131 3.181	2.942 2.942	2.968 2.971	2.959 2.962	2.959 2.986
(C2)	d = 50	3.135 3.142	3.277 3.270	2.942 2.942	2.938 2.933	2.956 2.960	2.936 2.953
(C3)	d = 100	3.206 3.207	3.412 3.423	2.953 2.942	2.959 2.954	2.957 2.964	2.948 2.933

3.5 Orthogonalized Within-Individual Statistic and Proposed Test

While each component, $Z_{\text{out},w}(t)$, $Z_{\text{out},d}(t)$, and $Z_{\text{in}}(t)$, captures a distinct aspect of distributional change, the analytical p-value of the combined statistic is complicated by the correlation between $Z_{\text{out},d}(t)$ and $Z_{\text{in}}(t)$. To address this issue, we construct an orthogonalized within-individual edge-count statistic that removes the linear dependence on $Z_{\text{out},d}(t)$, allowing for a simpler joint p-value approximation. Based on Lemma 1, let

$$\varrho = \text{Cov}(Z_{\text{out},d}(t), Z_{\text{in}}(t)) = \frac{\sum_{u=1}^{n} D_{uu} D_{u} - \frac{2}{n} |G_{\text{in}}| |G_{\text{out}}|}{\sqrt{\left(\sum_{u=1}^{n} D_{u}^{2} - \frac{4|G_{\text{out}}|^{2}}{n}\right) \left(\sum_{u=1}^{n} D_{uu}^{2} - \frac{|G_{\text{in}}|^{2}}{n}\right)}},$$
(10)

which is invariant with respect to t. We define the orthogonalized within-individual statistic as

$$Z_{\text{in},\perp}(t) = Z_{\text{in}}(t) - \varrho Z_{\text{out},d}(t)$$

with

$$\begin{split} \mathsf{E}(Z_{\mathrm{in},\perp}(t)) &= 0, \\ \mathsf{Var}(Z_{\mathrm{in},\perp}(t)) &= \mathsf{Var}(Z_{\mathrm{in}}(t)) - 2\varrho \, \mathsf{Cov}(Z_{\mathrm{out},d}(t),Z_{\mathrm{in}}(t)) + \varrho^2 \, \mathsf{Var}(Z_{\mathrm{out},d}(t)) \\ &= 1 - \varrho^2. \end{split}$$

Then the standardized version of $Z_{\text{in},\perp}(t)$ is obtained by

$$\tilde{Z}_{\rm in}(t) = \frac{Z_{\rm in,\perp}(t)}{\sqrt{1-\varrho^2}}.$$
(11)

Under Conditions 1–3, as $n \to \infty$, the sample correlation ϱ defined in (10) converges to its population counterpart. By construction, $\tilde{Z}_{\rm in}(t)$ is orthogonal to $Z_{{\rm out},d}(t)$, and since Theorem 4 states that ${\sf Cov}(Z_{\rm in}(s),Z_{{\rm out},w}(t))=0$ and ${\sf Cov}(Z_{{\rm out},w}(s),Z_{{\rm out},d}(t))=0$, we have ${\sf Cov}(\tilde{Z}_{\rm in}(s),Z_{{\rm out},w}(t))=0$ for all s,t. Hence, the processes $\{Z_{{\rm out},w}([nu]):0< u<1\}$, $\{|Z_{{\rm out},d}([nu])|:0< u<1\}$, and $\{|\tilde{Z}_{\rm in}([nu])|:0< u<1\}$ converge to mutually independent

Gaussian processes as $n \to \infty$. We denote $\{\tilde{Z}_{\text{in}}^*(u) : 0 < u < 1\}$ as the limiting Gaussian process corresponding to $\tilde{Z}_{\text{in}}([nu])$.

To derive the analytical p-value approximation, we examine the covariance structure of the proposed statistic. From Theorems 4 and 5, $Z_{\text{out},d}(\cdot)$ and $Z_{\text{in}}(\cdot)$ converge to zero-mean Gaussian processes with covariance kernels $\rho_{\text{out},d}(s,t)$ and $\rho_{\text{in}}(s,t)$, respectively, and their cross-covariance satisfies $\text{Cov}(Z_{\text{out},d}(s),Z_{\text{in}}(t)) = \varrho \, \rho_{\text{out},d}(s,t)$. Then we have

$$\operatorname{Cov}(\tilde{Z}_{\operatorname{in}}(s), \tilde{Z}_{\operatorname{in}}(t)) = \varrho \, \rho_{\operatorname{out},d}(s,t) = \varrho \, \rho_{\operatorname{in}}(s,t) \quad \forall s,t.$$

Consequently, $\mathsf{Cov}(\tilde{Z}^*_{\mathrm{in}}(u), \tilde{Z}^*_{\mathrm{in}}(v)) = \rho^*_{\mathrm{in}}(u, v) = \rho^*_{\mathrm{out}, d}(u, v).$

This result allows the analytical p-value for $|\tilde{Z}_{\rm in}(t)|$ to be derived in the same way as for $|Z_{{\rm out},d}(t)|$ and $|Z_{\rm in}(t)|$. The analytical p-value approximation after skewness correction for $|\tilde{Z}_{\rm in}(t)|$ is

$$\mathsf{P}\left(\max_{n_0 \le t \le n_1} |\tilde{Z}_{\rm in}(t)| > b\right) \approx 2b\phi(b) \int_{n_0/n}^{n_1/n} \tilde{K}_{\rm in}(nx) h_{\rm in}(n,x) \nu\left(b\sqrt{2h_{\rm in}(n,x)/n}\right) dx, \quad (12)$$

where $h_{in}(n,x)$ is defined in Remark 6 and

$$\begin{split} \tilde{K}_{\mathrm{in}}(t) &= \frac{\exp\left(\frac{1}{2}(b - \hat{\omega}_{b,\mathrm{in}}(t))^2 + \frac{1}{6}\tilde{\gamma}_{\mathrm{in}}(t)\hat{\omega}_{b,\mathrm{in}}(t)^3\right)}{\sqrt{1 + \gamma_{\mathrm{in}}(t)\hat{\omega}_{b,\mathrm{in}}(t)}}, \\ \hat{\omega}_{b,\mathrm{in}}(t) &= \frac{-1 + \sqrt{1 + 2\tilde{\gamma}_{\mathrm{in}}(t)b}}{\tilde{\gamma}_{\mathrm{in}}(t)}, \quad \tilde{\gamma}_{\mathrm{in}}(t) = \mathsf{E}(\tilde{Z}_{\mathrm{in}}^3(t)). \end{split}$$

 $\tilde{\gamma}_{\text{in}}(t)$ is computed from the third-order moments of $R_{\text{in},1}(t)$, $R_{\text{out},1}(t)$, and $R_{\text{out},2}(t)$. Specifically,

$$\mathsf{E}(\tilde{Z}_{\rm in}^3(t)) = \frac{\mathsf{E}(Z_{\rm in}^3(t)) - 3\varrho\,\mathsf{E}(Z_{\rm in}^2(t)Z_{{\rm out},d}(t)) + 3\varrho^2\,\mathsf{E}(Z_{\rm in}(t)Z_{{\rm out},d}^2(t)) - \varrho^3\,\mathsf{E}(Z_{{\rm out},d}^3(t))}{\sqrt{(1-\varrho^2)^3}}$$

with

$$\begin{split} \mathsf{E}(Z_{\text{in}}^2(t)Z_{\text{out},d}(t)) &= \frac{\mathsf{E}(R_{\text{in},1}^2(t)R_{\text{out},d}(t)) - 2\mu_{\text{in}}(t)\mathsf{E}(R_{\text{in},1}(t)R_{\text{out},d}(t)) - 2\mu_{\text{out},d}(t)\mathsf{E}(R_{\text{in},1}^2(t)) + 3\mu_{\text{in}}^2(t)\mu_{\text{out},d}(t)}{\sigma_{\text{in}}^2(t)\sigma_{\text{out},d}(t)}, \\ \mathsf{E}(Z_{\text{in}}(t)Z_{\text{out},d}^2(t)) &= \frac{\mathsf{E}(R_{\text{in},1}(t)R_{\text{out},d}^2(t)) - 2\mu_{\text{out},d}(t)\mathsf{E}(R_{\text{in},1}(t)R_{\text{out},d}(t)) - 2\mu_{\text{in}}(t)\mathsf{E}(R_{\text{out},d}^2(t)) + 3\mu_{\text{in}}(t)\mu_{\text{out},d}^2(t)}{\sigma_{\text{in}}(t)\sigma_{\text{out},d}^2(t)}. \end{split}$$

The remaining quantities are $\mathsf{E}(R_{\mathrm{in}}^2(t)R_{\mathrm{out},d}(t))$ and $\mathsf{E}(R_{\mathrm{in}}(t)R_{\mathrm{out},d}^2(t))$, whose analytic forms are provided in Appendix ??.

The corresponding critical values for $|Z_{\rm in}(t)|$ obtained from the same dataset as in Tables 1 and 2, are summarized in Table 3. These results are almost the same as the critical values for $|Z_{\rm in}(t)|$.

We then propose a final max-type edge-count statistic, which can be expressed as

$$M(t) = \max \left\{ Z_{\text{out},w}(t), |Z_{\text{out},d}(t)|, |\tilde{Z}_{\text{in}}(t)| \right\}, \tag{13}$$

Table 3: Critical values of $|\tilde{Z}_{\rm in}(t)|$ at 0.05 significance level. $n=200,\ \ell=5.$

(a) $n_0 = 0.05n$				(b) n_0	= 0.1n		
	A1 :	3.032				A1	2.942
		A2	Per		·		A2
(C1)	d = 10	3.074 3.073	3.107 3.076	(C1)	_	d = 10	2.959 2.961
C2)	d = 50	3.062 3.073	3.030 3.107	(C2)	_	d = 50	2.956 2.960
C3)	d = 100	3.091 3.064	3.103 3.041	(C3)	_	d = 100	2.956 2.964

and the corresponding scan statistic

$$\max_{n_0 \le t \le n_1} M(t). \tag{14}$$

We reject H_0 when the scan statistic (14) exceeds the critical value at the pre-specified significance level. To obtain this critical value, we compute the corresponding p-value p_M under the permutation null. The p-value is determined from the tail probability of the max-type scan statistic, which can be expressed as

$$P\left(\max_{n_0 \le t \le n_1} M(t) > b\right)$$

$$= 1 - P\left(\max_{n_0 \le t \le n_1} Z_{\text{out},w}(t) < b\right) P\left(\max_{n_0 \le t \le n_1} |Z_{\text{out},d}(t)| < b\right) P\left(\max_{n_0 \le t \le n_1} |\tilde{Z}_{\text{in}}(t)| < b\right). \tag{15}$$

The approximations for the constituent scan statistics are directly given (7), (8), and (12). The proposed test is summarized in Algorithm 1.

Algorithm 1 The new test

Require: A sequence of observations $\{y_i\}_{i=1,\dots,n}$ and the significance level α .

Ensure: Reject the null hypothesis H_0 (1) if p_M (15) is less than α . The location of the change-point is estimated using (14).

- 1: Construct the similarity graph G (e.g., 9-MST) on the sequence of observations with repeated measurements.
- 2: Compute the scan statistic (14) based on Lemma 1 and (11).
- 3: Obtain p_M from (7), (8), and (12).

4 Simulation Study

We examine the performance of the new test under various simulation settings. We consider the observed data generated as follows:

- Multivariate Gaussian: $Z_{ij} \stackrel{\text{ind.}}{\sim} N_d(\theta_{ij}, \omega_i^2 I_d)$.
- Multivariate log-normal: $Z_{ij} \stackrel{\text{ind.}}{\sim} \text{Lognormal}_d(\theta_{ij}, \omega_i^2 I_d)$.
- Multivariate Gaussian mixture: $Z_{ij} \stackrel{\text{ind.}}{\sim} W \cdot N_d(\theta_{ij}, \omega_i^2 I_d) + (1 W)N_d(\theta_{ij} + 2, 0.5 \cdot \omega_i^2 I_d), \quad W \sim Bernoulli(0.5).$

with mean vectors $(\theta_{i1}^T, \dots, \theta_{i\ell}^T) \mid \mu_{ki} \sim N_{d\ell}(\mu_{ki}, \sigma^2 \varrho_k \otimes I_d)$ where $\mu_{ki} = (a_{ki}^T, \dots, a_{ki}^T)^T$, $a_{ki} \stackrel{\text{i.i.d.}}{\sim} N_d(\beta_k, \epsilon_k^2 I_d)$ and $\varrho_k = \rho_k \mathbf{1}_\ell \mathbf{1}_\ell^T + (1 - \rho_k) I_\ell$, and covariance parameter $\omega_i \stackrel{\text{i.i.d.}}{\sim} U(\nu_{k1}, \nu_{k2})$ for $j = 1, \dots, \ell$, $i = 1, \dots, n$. The index k is set to 1 if the observation time is at or before the true change-point τ , and set to 2 if it is after τ . Here, \otimes denotes the Kronecker product.

We compare the new method with two existing methods, the generalized edge-count change-point detection by Chu and Chen (2019), the Fréchet change-point detection by Dubey and Müller (2020) and two recent machine learning approaches, changeforest and changekNN by Londschien et al. (2023). To ensure a fair evaluation for repeated measures data, we aggregate the information from repeated measurements using two distance metrics. In the first approach, each individual's repeated measurements are averaged so that the distance is computed as

$$d(y_i, y_{i'}) = d(\tilde{y}_i, \tilde{y}_{i'})$$
 where $\tilde{y}_i = \frac{1}{\ell} \sum_{j=1}^{\ell} y_{ij}, \ \tilde{y}_{i'} = \frac{1}{\ell} \sum_{j=1}^{\ell} y_{i'j}$

for any individuals $i \neq i'$, where each y_{ij} is a d-dimensional observation. The second approach uses the integrated distance

$$d(y_i, y_{i'}) = \sqrt{\sum_{j=1}^{\ell} \|y_{ij} - y_{i'j}\|^2},$$

treating each repeated measure as a feature and pooling the ℓ repeated measurements into $\ell \times d$ dimensions. We denote the generalized edge-count change-point detection, the Fréchet change-point detection, the changeforest, and the changekNN applied with the first approach as S_1 , Fréchet₁, changeforest₁, and changekNN₁ respectively, and with the second approach as S_2 , Fréchet₂, changeforest₂, and changekNN₂. The new test is denoted M.

We simulate 100 sequences with n=100 and $\ell=5$, and set the true change-point to $\tau=50$. The similarity graph G is constructed using the 9-MST. We consider dimensions d=40 and d=50. By varying parameters $\rho, \beta, \epsilon, \nu_{..}, \sigma$, we define four settings. Setting 1 represents the null hypothesis with no change-point. Setting 2 introduces within-individual differences. Setting 3 has the location change between individuals, while Setting 4 changes between-individual scale. The specific parameter values for each setting are listed in Table 4.

Table 5 reports the number of rejections at 5% significance level out of 100 replicates for the multivariate Gaussian data. The numbers in parentheses indicate how often the estimated change-point falls within [40, 60] around the true change-point 50. Under the null (Setting 1), most of tests successfully control the type I error rate. In the presence of within-individual differences (Setting 2), the proposed test M consistently detects changes with

Table 4: Simulation settings for the multivariate Gaussian, log-normal, and Gaussian mixture scenarios with parameters. $\sigma=1$. Each parenthesis shows parameters for k=1 (left) and k=2 (right). $\mathbf{0}_d$ and $\mathbf{1}_d$ denote the d-dimensional zero and one vectors, respectively.

Setting	ρ	β	ϵ	$ u_{.1} $	$ u_{.2} $
Gaussian					
Setting 1 (Null) Setting 2 (Within-diff.) Setting 3 (Between-diff. of location) Setting 4 (Between-diff. of scale)	$ \begin{array}{c} (0.2, 0.2) \\ (0.1, 0.3) \\ (0.2, 0.2) \\ (0.2, 0.2) \end{array} $	$egin{aligned} (0_d, 0_d) \ (0_d, 0_d) \ (0_d, 0.3 \cdot 1_d) \ (0_d, 0_d) \end{aligned}$	(1,1) $(1,1)$ $(1,1)$ $(1,1,1)$	(1,1) $(1,1)$ $(1,1)$ $(1,1,1)$	$ \begin{array}{c} (1.2, 1.2) \\ (1.2, 1.2) \\ (1.2, 1.2) \\ (1.1, 1.2) \end{array} $
Log-normal					
Setting 1 (Null) Setting 2 (Within-diff.) Setting 3 (Between-diff. of location) Setting 4 (Between-diff. of scale)	$ \begin{array}{c} (0.2, 0.2) \\ (0.1, 0.6) \\ (0.2, 0.2) \\ (0.2, 0.2) \end{array} $	$egin{aligned} (0_d, 0_d) \ (0_d, 0_d) \ (0_d, 0.4 \cdot 1_d) \ (0_d, 0_d) \end{aligned}$	(1,1) $(1,1)$ $(1,1)$ $(1,1.2)$	(1,1) $(1,1)$ $(1,1)$ $(1,1.2)$	(1.2, 1.2) (1.2, 1.2) (1.2, 1.2) (1.1, 1.3)
Gaussian mixture					
Setting 1 (Null) Setting 2 (Within-diff.) Setting 3 (Between-diff. of location) Setting 4 (Between-diff. of scale)	(0.2, 0.2) (0.1, 0.4) (0.2, 0.2) (0.2, 0.2)	$egin{array}{c} (0_d, 0_d) \\ (0_d, 0_d) \\ (0_d, 0.45 \cdot 1_d) \\ (0_d, 0_d) \end{array}$	(1,1) $(1,1)$ $(1,1)$ $(1,1.1)$	(1,1) $(1,1)$ $(1,1)$ $(1,1.2)$	(1.2, 1.2) (1.2, 1.2) (1.2, 1.2) (1.1, 1.3)

Table 5: Number of rejections at 5% significance level (out of 100 replicates) for the multivariate Gaussian data, with the number of detected change-points within [40, 60] in parentheses.

_		Setting 1	Setting 2	Setting 3	Setting 4
	M	2	74(56)	62(51)	79(73)
	S_1	7	16(8)	74(62)	49(29)
	S_2	4	3(0)	61(50)	89(76)
	$Fr\'echet_1$	4	0(0)	12(6)	9(6)
d = 40	$Fr\'echet_2$	1	0(0)	2(0)	0(0)
	$change forest_1$	3	9(1)	79(69)	9(1)
	${\it change} {\it forest}_2$	3	5(2)	47(35)	10(2)
	${\rm changekNN_1}$	9	5(0)	58(38)	2(0)
	${\rm changekNN}_2$	4	6(0)	55(35)	2(0)
	M	6	82(72)	68(58)	80(62)
	S_1	4	23(12)	77(59)	47(29)
	S_2	7	2(1)	63(53)	90(73)
	$Fr\'echet_1$	1	2(0)	16(7)	4(2)
d = 50	$Fr\'echet_2$	0	0(0)	1(0)	1(1)
	$change forest_1$	5	8(3)	78(67)	18(8)
	${\rm change forest}_2$	8	4(0)	55(39)	7(1)
	${\rm changekNN}_1$	12	2(0)	61(35)	6(0)
	${\rm changekNN}_2$	3	5(0)	49(26)	3(0)

high accuracy, while other methods do not work well. For between-individual differences in Settings 3 and 4, all methods exhibit comparable power; changeforest₁ and S_1 attain the highest power in Setting 3, whereas S_2 outperforms others in Setting 4. Because S_2 pools the data into $\ell \times d$ dimensions, it tends to require longer computation time than the other tests. The Fréchet-based methods perform poorly when the parameter differences between observations before and after the change-point are small. The changeforest and changekNN methods achieve high performance under Setting 3, but they fail to detect changes effectively in Settings 2 and 4. As is typical for graph-based CPD, we observe that test power generally improves as the dimension increases. Overall, M is the only method that reliably detects within-individual differences while still performing well to detect between-individual location and scale changes, making the new test promising when within-individual structure matters.

Table 6: Results for the multivariate log-normal data.

		Setting 1	Setting 2	Setting 3	Setting 4
	M	2	78(67)	94(76)	92(78)
	S_1	5	4(0)	88(74)	91(77)
	S_2	5	6(1)	52(36)	65(51)
	$Fr\'echet_1$	9	5(0)	27(10)	37(16)
d = 40	$Fr\'echet_2$	7	4(0)	25(7)	39(14)
	$change forest_1$	5	25(13)	95(94)	30(14)
	${\it change} {\it forest}_2$	2	11(2)	87(79)	29(12)
	${\rm changekNN}_1$	4	4(0)	13(0)	14(0)
	${\rm changekNN}_2$	5	5(0)	6(0)	10(0)
	M	4	90(81)	95(85)	97(85)
	S_1	7	6(1)	82(70)	89(75)
	S_2	4	11(2)	37(19)	55(35)
	$Fr\'echet_1$	6	3(0)	14(9)	35(19)
d = 50	$Fr\'echet_2$	4	6(0)	13(6)	30(12)
	$change forest_1$	11	37(14)	98(94)	29(15)
	$change forest_2$	8	8(3)	82(75)	26(10)
	${\rm changekNN_1}$	6	8(0)	17(0)	13(0)
	${\rm changekNN}_2$	4	3(0)	6(0)	4(0)

Tables 6 and 7 present the results for the multivariate log-normal and the multivariate Gaussian mixture data, respectively. The overall patterns are similar to those in Table 5 for the Gaussian case. Across both distributions, the proposed test M exhibits strong performance in detecting within-individual differences (Setting 2) and also performs competitively for between-individual location (Setting 3) and scale (Setting 4) changes.

5 Real Data Analysis

To evaluate the proposed method in a real-world setting, we apply it to the NYC Taxi dataset provided by the New York City taxi and Limousine Commission (TLC). The dataset is publicly available at https://www.nyc.gov/site/tlc/about/tlc-trip-record-data.page. We use taxi trip records where passengers were picked up at John F. Kennedy (JFK)

Table 7: Results for the multivariate Gaussian mixture data.

		Setting 1	Setting 2	Setting 3	Setting 4
	M	3	78(73)	83(74)	90(78)
	S_1	3	31(22)	94(90)	46(37)
	S_2	5	6(2)	81(74)	99(90)
	$Fr\'echet_1$	7	7(1)	29(10)	8(1)
d = 40	$Fr\'echet_2$	5	5(1)	23(6)	7(1)
	$change forest_1$	6	12(6)	30(19)	11(5)
	$change for est_2$	10	7(1)	20(13)	14(5)
	${\rm changekNN}_1$	8	7(0)	98(89)	6(0)
	${\rm changekNN}_2$	6	3(0)	93(83)	2(0)
	M	6	80(72)	94(90)	95(85)
	S_1	6	36(25)	97(92)	59(46)
	S_2	9	8(2)	89(81)	100(91)
	$Fr\'echet_1$	3	3(0)	23(13)	5(1)
d = 50	$Fr\'echet_2$	1	3(0)	23(13)	3(1)
	$change forest_1$	4	6(2)	31(17)	7(3)
	$change forest_2$	7	9(1)	16(10)	12(4)
	$\operatorname{changekNN}_1$	5	3(0)	96(88)	4(0)
	${\rm changekNN}_2$	7	3(0)	94(83)	5(0)

International Airport and dropped off anywhere in New York City. To preprocess the data, we first filter all trips that originated from the JFK area. We then divide the New York City area near JFK Airport into a 30 by 30 grid based on longitude and latitude, and construct a matrix of taxi drop-off counts within each cell for each day. Each daily matrix is log-transformed to stabilize large counts. The boundary of this area is set to latitude 40.63 to 40.66 and longitude -73.80 to -73.77. We consider the time period from January 4, 2015 to February 27, 2016, comprising a total of 60 weeks with 420 days. To reflect weekly travel patterns, we treat each day as a repeated measurement and test for a significant change-point across the 60 weekly observations. Figure 4 shows heatmaps of taxi drop-offs for two example days.

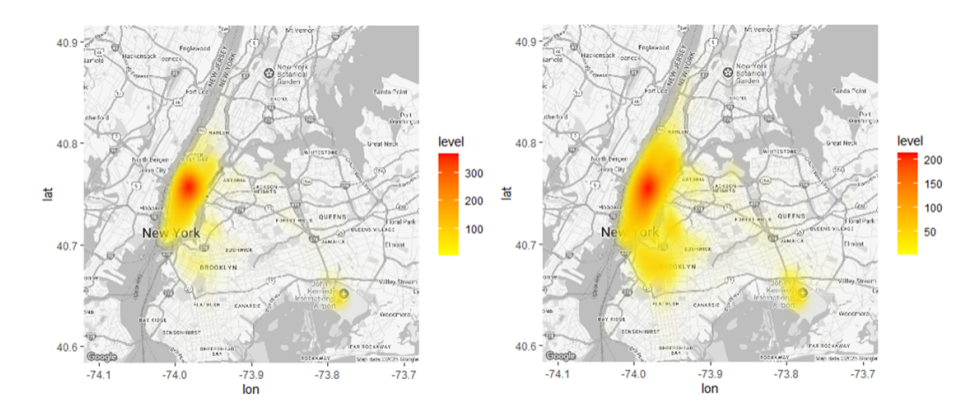


Figure 4: Density heatmaps of taxi drop-offs on Dec 1 (left) and Dec 31 (right), 2015.

The estimated change-points are listed in Table 8. The change-points are estimated using a recursive binary segmentation procedure, which detects all possible change-points at the 5% significance level. The proposed test M detects four major periods of change, specifically early February (Lunar New Year), late March (Spring Break), late October (Halloween Day), and mid-December (Christmas). These change-points correspond to meaningful events or holidays that plausibly affect NYC taxi movements, but some of these periods are not identified by the competing methods. Similarly, changekNN₁ detects a comparable set of events, while other methods such as S_1 and S_2 detect changes only within specific periods such as the spring, fall, and Halloween seasons. Table 9 summarizes the p-values of the constituent statistics below the 5% level. Each change-point of M is supported by at least one significant component statistic, showing that the test draws on both between-individual and within-individual variations.

Table 8: Detected change-points results in NYC taxi movements.

Method	Week	Date	Event
	5	2015.2.1-2015.2.7	Lunar New Year
M	12	2015.3.22-2015.3.28	Spring Break
IVI	43	2015.10.25-2015.10.31	Halloween Day
	50	2015.12.13-2015.12.19	Christmas
	12	2015.3.22-2015.3.28	Spring Break
S_1	35	2015.8.30-2015.9.5	Beginning of Fall Semester
	43	2015.10.25-2015.10.31	Halloween Day
S_2	13	2015.3.29–2015.4.4	Spring Break
S_2	43	2015.10.25-2015.10.31	Halloween Day
$Fr\'echet_1$	43	2015.10.25-2015.10.31	Halloween Day
Fréchet ₂	_	_	_
	13	2015.3.29–2015.4.4	Spring Break
$change forest_1$	27	2015.7.5–2015.7.11	Summer Break
	42	2015.10.18-2015.10.24	Halloween Day
$change for est_2$	19	2015.5.10-2015.5.16	End of Spring Semester
${\rm changekNN}_1$	29	2015.7.19-2015.7.25	Summer Break
	6	2015.2.8–2015.2.14	Lunar New Year
changekNN ₂	12	2015.3.22-2015.3.28	Spring Break
changekiviv ₂	45	2015.11.8–2015.11.14	Thanksgiving
	53	2016.1.3-2016.1.9	Christmas & New Year

Table 9: Significant constituent statistics for each detected change-point by M.

Week	$Z_{\mathrm{out},w}(t)$	$ Z_{\mathrm{out},d}(t) $	$ \tilde{Z}_{\mathrm{in}}(t) $
5	_	0.023	_
12	0.001	0.009	_
43	0.000	_	0.012
50	0.028	0.022	_

6 Discussion

In this paper, we propose the new graph-based change-point framework tailored to a sequence with repeated measurements or local structures. We construct scan statistics that capture both within-individual and between-individual changes and combine them via a max-type strategy. We establish the limiting distributions and provide accurate, scalable inference through analytical p-value approximations with skewness correction, while also offering the permutation-based option when desired.

The proposed test leverages within-individual information when repeated measurements are available. The framework can be further extended to relax assumptions on repeated-measure structures. In practice, the number of repeated measures ℓ may vary across individuals, rather than being fixed. Various types of shifts may also arise within individuals, just as we considered both location and scale shifts in the between-individual setting. Future work may focus on developing more flexible CPD procedures that accommodate varying numbers of repeated measures and a broader class of within-individual changes.

The new procedures identify the most prominent single change-point in a sequence. When multiple changes are present, they can be applied recursively alongside techniques, such as binary segmentation, wild binary segmentation, or seeded binary segmentation (Vostrikova, 1981; Fryzlewicz et al., 2014; Kovács et al., 2023).

Acknowledgments and Disclosure of Funding

This research is supported, in part, by KAIST Starting Fund (KAIST-G04240003) and National Research Foundation of Korea (RS-2022-NR068758).

References

Farzaneh Ahmadzadeh. Change point detection with multivariate control charts by artificial neural network. The International Journal of Advanced Manufacturing Technology, 97 (9):3179–3190, 2018.

Samaneh Aminikhanghahi and Diane J Cook. A survey of methods for time series change point detection. *Knowledge and information systems*, 51(2):339–367, 2017.

Edward G Carlstein, David Siegmund, et al. Change-point problems. IMS, 1994.

Hao Chen and Jerome H Friedman. A new graph-based two-sample test for multivariate and object data. *Journal of the American statistical association*, 112(517):397–409, 2017.

Hao Chen and Nancy Zhang. Graph-based change-point detection. 2015.

Hao Chen, Xu Chen, and Yi Su. A weighted edge-count two-sample test for multivariate and object data. *Journal of the American Statistical Association*, 113(523):1146–1155, 2018.

Jie Chen, Arjun K Gupta, and AK Gupta. Parametric statistical change point analysis, volume 192. Springer, 2000.

- Lynna Chu and Hao Chen. Asymptotic distribution-free change-point detection for multivariate and non-euclidean data. *The Annals of Statistics*, 47(1):382–414, 2019.
- Frédéric Desobry, Manuel Davy, and Christian Doncarli. An online kernel change detection algorithm. *IEEE Transactions on Signal Processing*, 53(8):2961–2974, 2005.
- Paromita Dubey and Hans-Georg Müller. Fréchet change-point detection. *The Annals of Statistics*, 48(6):3312–3335, 2020.
- Piotr Fryzlewicz et al. Wild binary segmentation for multiple change-point detection. *The Annals of Statistics*, 42(6):2243–2281, 2014.
- Zaid Harchaoui, Eric Moulines, and Francis Bach. Kernel change-point analysis. Advances in neural information processing systems, 21, 2008.
- Lajos Horváth and Marie Hušková. Change-point detection in panel data. *Journal of Time Series Analysis*, 33(4):631–648, 2012.
- Baihong Jin, Yuxin Chen, Dan Li, Kameshwar Poolla, and Alberto Sangiovanni-Vincentelli. A one-class support vector machine calibration method for time series change point detection. In 2019 IEEE International conference on prognostics and health management (ICPHM), pages 1–5. IEEE, 2019.
- Solt Kovács, Peter Bühlmann, Housen Li, and Axel Munk. Seeded binary segmentation: a general methodology for fast and optimal changepoint detection. *Biometrika*, 110(1): 249–256, 2023.
- Jae Won Lee and David L Demets. Sequential comparison of changes with repeated measurements data. *Journal of the American Statistical Association*, 86(415):757–762, 1991.
- Jie Li, Paul Fearnhead, Piotr Fryzlewicz, and Tengyao Wang. Automatic change-point detection in time series via deep learning. *Journal of the Royal Statistical Society Series B: Statistical Methodology*, 86(2):273–285, 2024.
- Jun Li. Asymptotic distribution-free change-point detection based on interpoint distances for high-dimensional data. *Journal of Nonparametric Statistics*, 32(1):157–184, 2020.
- Shuang Li, Yao Xie, Hanjun Dai, and Le Song. M-statistic for kernel change-point detection. Advances in Neural Information Processing Systems, 28, 2015.
- F Lombard. Rank tests for changepoint problems. Biometrika, 74(3):615–624, 1987.
- Malte Londschien, Peter Bühlmann, and Solt Kovács. Random forests for change point detection. *Journal of Machine Learning Research*, 24(216):1–45, 2023.
- David S Matteson and Nicholas A James. A nonparametric approach for multiple change point analysis of multivariate data. *Journal of the American Statistical Association*, 109 (505):334–345, 2014.
- Anthony N Pettitt. A non-parametric approach to the change-point problem. *Journal of the Royal Statistical Society: Series C (Applied Statistics)*, 28(2):126–135, 1979.

- Gordon J Ross and Niall M Adams. Two nonparametric control charts for detecting arbitrary distribution changes. *Journal of Quality Technology*, 44(2):102–116, 2012.
- Yunus Saatçi, Ryan D Turner, and Carl E Rasmussen. Gaussian process change point models. In *Proceedings of the 27th International Conference on Machine Learning (ICML-10)*, pages 927–934, 2010.
- Xiaoping Shi, Yuehua Wu, and Calyampudi Radhakrishna Rao. Consistent and powerful graph-based change-point test for high-dimensional data. *Proceedings of the National Academy of Sciences*, 114(15):3873–3878, 2017.
- D Siegmund. Tail approximations for maxima of random fields. In *Probability Theory:* Proceedings of the 1989 Singapore Probability Conference, pages 147–158. Singapore, 1992.
- David Siegmund. Approximate tail probabilities for the maxima of some random fields. *The Annals of Probability*, pages 487–501, 1988.
- David Siegmund and Benjamin Yakir. The statistics of gene mapping. Springer, 2007.
- Hoseung Song and Hao Chen. Asymptotic distribution-free changepoint detection for data with repeated observations. *Biometrika*, 109(3):783–798, 2022.
- Hoseung Song and Hao Chen. Practical and powerful kernel-based change-point detection. *IEEE Transactions on Signal Processing*, 2024.
- Ju L Vostrikova. Detecting disorder in multidimensional random process. In *Soviet Math. Dokl*, volume 24, pages 55–59, 1981.
- Heng Wang, Minh Tang, Youngser Park, and Carey E Priebe. Locality statistics for anomaly detection in time series of graphs. *IEEE Transactions on Signal Processing*, 62(3):703–717, 2013.
- Michael Woodroofe. Frequentist properties of bayesian sequential tests. *Biometrika*, 63(1): 101–110, 1976.
- Michael Woodroofe. Large deviations of likelihood ratio statistics with applications to sequential testing. *The Annals of Statistics*, pages 72–84, 1978.
- Jingru Zhang, Kathleen R Merikangas, Hongzhe Li, and Haochang Shou. Two-sample tests for multivariate repeated measurements of histogram objects with applications to wearable device data. The annals of applied statistics, 16(4):2396, 2022.
- Doudou Zhou and Hao Chen. Asymptotic distribution-free change-point detection for modern data based on a new ranking scheme. *IEEE Transactions on Information Theory*, 2025.